ACS Energy LETTERS

http://pubs.acs.org/journal/aelccp

Single Rh Adatoms Stabilized on α-$Fe_2O_3(1\bar{1}02)$ by Coadsorbed Water

Florian Kraushofer, Lena Haager, Moritz Eder, Ali Rafsanjani-Abbasi, Zdeněk Jakub, Giada Franceschi, Michele Riva, Matthias Meier, Michael Schmid, Ulrike Diebold, and Gareth S. Parkinson*

Cite This: *ACS Energy Lett.* 2022, 7, 375–380

Read Online

ACCESS | Metrics & More | Article Recommendations | Supporting Information

ABSTRACT: **Oxide-supported single-atom catalysts are commonly modeled as a metal atom substituting surface cation sites in a low-index surface. Adatoms with dangling bonds will inevitably coordinate molecules from the gas phase, and adsorbates such as water can affect both stability and catalytic activity. Herein, we use scanning tunneling microscopy (STM), noncontact atomic force microscopy (ncAFM), and X-ray photoelectron spectroscopy (XPS) to show that high densities of single Rh adatoms are stabilized on α-$Fe_2O_3(1\bar{1}02)$ in the presence of 2×10^{-8} mbar of water at room temperature, in marked contrast to the rapid sintering observed under UHV conditions. Annealing to 50 °C in UHV desorbs all water from the substrate leaving only the OH groups coordinated to Rh, and high-resolution ncAFM images provide a direct view into the internal structure. We provide direct evidence of the importance of OH ligands in the stability of single atoms and argue that their presence should be assumed when modeling single-atom catalysis systems.**

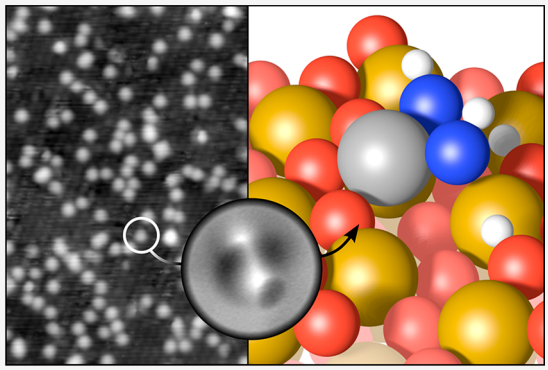

Understanding how metals bind to oxide supports has long been a goal of catalysis research. The issue is particularly pressing in the field of single-atom catalysis (SAC), because the coordination environment of the active site not only decides whether the metal atoms will be stable against thermal sintering but also strongly affects the catalytic properties. Because transmission electron microscopy (TEM) studies usually assign the isolated adatoms to be located in cation-like sites relative to the bulk structure,[1−7] bulk-continuation or substitutional sites are commonly used as a starting point for exploring reaction pathways.[1,8−11] A more realistic model would account for the extensive hydroxylation of the support that usually occurs in reactive environments, but given the difficulty ascertaining reliable information on the local structure from experiment, this additional complexity is usually omitted. It can be important, however, as coordinating additional OH to Rh adatoms has been shown to strongly affect the binding energy of CO at that site,[12] and adsorbed water can play a direct role in catalytic mechanisms.[13,14]

Herein, we explore the stability of single Rh adatoms on hematite (α-Fe_2O_3), with and without the presence of water. While the α-$Fe_2O_3(0001)$ surface is commonly used to represent FeO_x catalysts in computations,[1,8−11] it is a poor choice for a model system because the atomic-scale structure is unclear even under UHV conditions.[15,16] We instead utilize the $(1\bar{1}02)$ facet, on which a monophase bulk-truncated (1×1) termination can reproducibly be prepared.[17−20] Moreover, the surface structure and its interaction with water are well-understood.[17,18] The surface termination[17] and room-temperature water adsorption sites[18] are introduced in Figure S1. We show that isolated Rh atoms form only in the presence of water vapor; rapid sintering occurs already at room temperature in UHV conditions. The stabilization occurs through the coordination of multiple OH ligands, which remain on the surface at 50 °C after all other water has desorbed.

Figure 1 shows STM data taken after depositing Rh on the α-$Fe_2O_3(1\bar{1}02)$ surface in UHV and in a partial pressure of 2×10^{-8} mbar H_2O. In the case of room-temperature deposition in UHV (Figure 1a), this surface does not stabilize single Rh adatoms, which instead form small clusters after deposition.[20] In contrast, after depositing with background H_2O, the majority of features in Figure 1b,c appear as uniform isolated protrusions. To determine how many Rh atoms each feature contains, we performed a separate experiment in which we again deposited Rh in background H_2O, evaluated the

Received: November 4, 2021
Accepted: December 17, 2021
Published: December 22, 2021

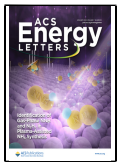

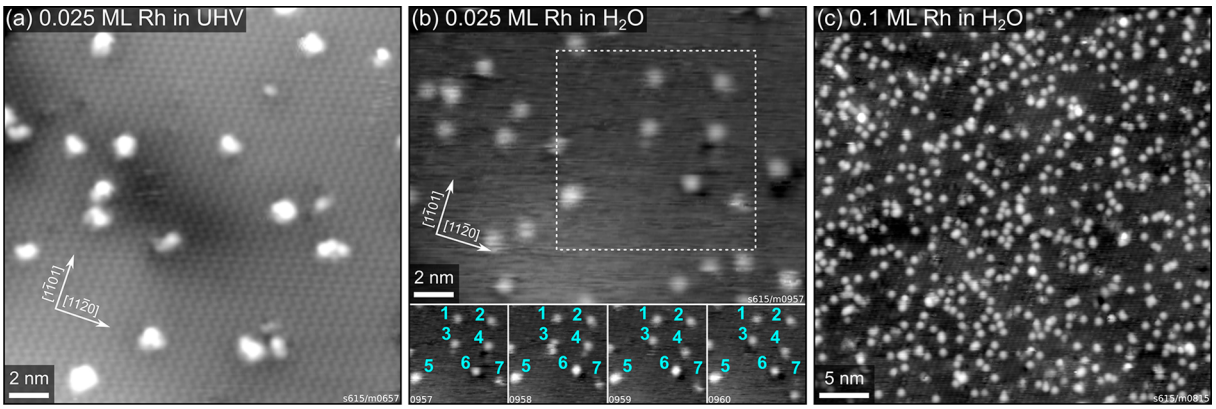

Figure 1. Rh stabilization by H_2O on α-$Fe_2O_3(1\bar{1}02)$. (a) STM image (U_{sample} = +3 V, I_{tunnel} = 0.3 nA) of 0.025 ML Rh on α-$Fe_2O_3(1\bar{1}02)$, deposited at room temperature in UHV. (b) STM image (U_{sample} = +3 V, I_{tunnel} = 0.2 nA) of 0.025 ML Rh on α-$Fe_2O_3(1\bar{1}02)$, deposited at room temperature in a background of 2×10^{-8} mbar H_2O. Consecutive STM images from the area indicated by the dashed square are shown in the bottom row, with the same features labeled in cyan in each frame. (c) STM image (U_{sample} = +2 V, I_{tunnel} = 0.3 nA) of 0.1 ML Rh on α-$Fe_2O_3(1\bar{1}02)$, deposited in a partial pressure of 2×10^{-8} mbar H_2O.

feature density in STM, then annealed the surface in oxygen at 520 °C. We have shown previously that this results in Rh being incorporated in the first subsurface layer,[20] where it is still imaged as well-defined, isolated features in STM, without significant loss of Rh to the bulk. Because the same density of features was found before and after incorporation (shown in Figure S3 and corresponding text), we assign the bright features in Figure 1b,c as single Rh adatoms stabilized by water.

At low Rh coverage, the features are occasionally mobile, as can be seen in consecutive STM images taken from the same area. In the four frames shown in Figure 1b, the features labeled as 3, 4, and 7 move over the course of the acquisition, while the rest remain in place. Furthermore, we observe that some of the features appear brighter than the majority, but that they can switch between the two apparent heights from one frame to the next. This is the case for the feature labeled as 6 in Figure 1b, which appears brighter in the second and third frames. The two different apparent heights are measured as (108 ± 6) pm and (223 ± 13) pm with respect to the water-covered substrate. Despite the mobility of the features, no agglomeration to clusters was observed. This suggests that the adatoms are stabilized thermodynamically instead of kinetically, i.e., diffusion barriers are low, but it is energetically favorable to keep the atoms separated in the presence of water.

XPS data of the O 1s region corresponding to the STM images in Figure 1b,c are shown in Figure 2. The main contribution at 529.9 eV is assigned to lattice oxygen, and two additional contributions at 532.9 and 531.5 eV are assigned to molecular H_2O and OH groups, respectively.[18] It is worth noting that in both cases, the O 1s peak contains a significantly higher fraction of OH in the presence of Rh than on the pristine surface. In the absence of rhodium, the H_2O/OH ratio is consistently about 0.40 for any submonolayer water coverage.[18] Because dissociation results in two hydroxy groups per H_2O, this ratio corresponds to 45% of the water being molecularly adsorbed. Instead, in the presence of Rh, we find an H_2O/OH ratio of 0.32 for 0.025 ML Rh and of only 0.17 for 0.1 ML Rh. In terms of how much water is molecularly adsorbed, this would correspond to only 39% and 26%, respectively. Thus, more water is clearly being dissociated with increasing Rh coverage, which suggests that Rh atoms are active sites for water dissociation. XPS C 1s data was also

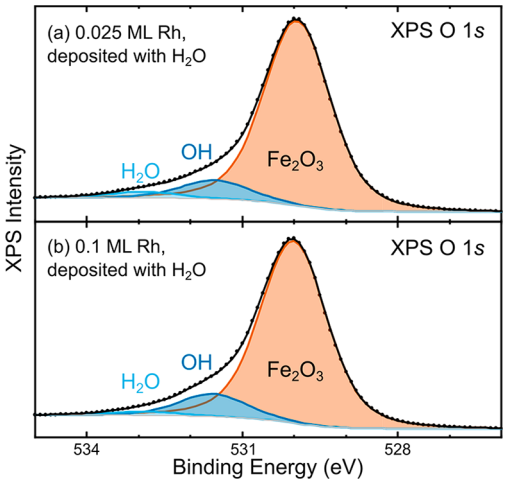

Figure 2. O 1s region in XPS (Al Kα, 70° grazing emission, pass energy 16 eV) of Rh stabilized by H_2O on α-$Fe_2O_3(1\bar{1}02)$. Spectra for (a) 0.025 ML and (b) 0.1 ML Rh deposited in 2×10^{-8} mbar H_2O correspond to the STM images in panels b and c of Figure 1. The data (black points) were fitted (solid lines) with a component corresponding to lattice O^{2-} anions at 529.9 eV and contributions from molecular H_2O (532.9 eV) and OH (531.5 eV).[18]

routinely collected on the pristine surface, after Rh deposition and after annealing. We found no sign of contamination within the detection limit of the instrument (<0.01 ML carbon atoms), allowing us to rule out contributions of carbonaceous species to the O 1s spectra.

To investigate the thermal stability of water-stabilized Rh adatoms, we performed consecutive heating steps after deposition of 0.025 ML Rh in 2×10^{-8} mbar water. After each step, the sample was cooled to room temperature to acquire XPS and STM data (shown in Figure 3). The O 1s peak (Figure 3a) shifts to higher binding energy by 0.2 eV immediately after deposition, most likely because of band bending caused by the adsorbates. The component corresponding to H_2O (532.9 eV) disappears after annealing at 50 °C for 10 min, but a small shoulder corresponding to OH (531.5 eV) remains, accounting for 1.2% of the O 1s peak area. Fits to the data are shown in Figure S2. The OH peak area further decreases to 0.5% of the total O 1s peak area when

https://doi.org/10.1021/acsenergylett.1c02405
ACS Energy Lett. 2022, 7, 375−380

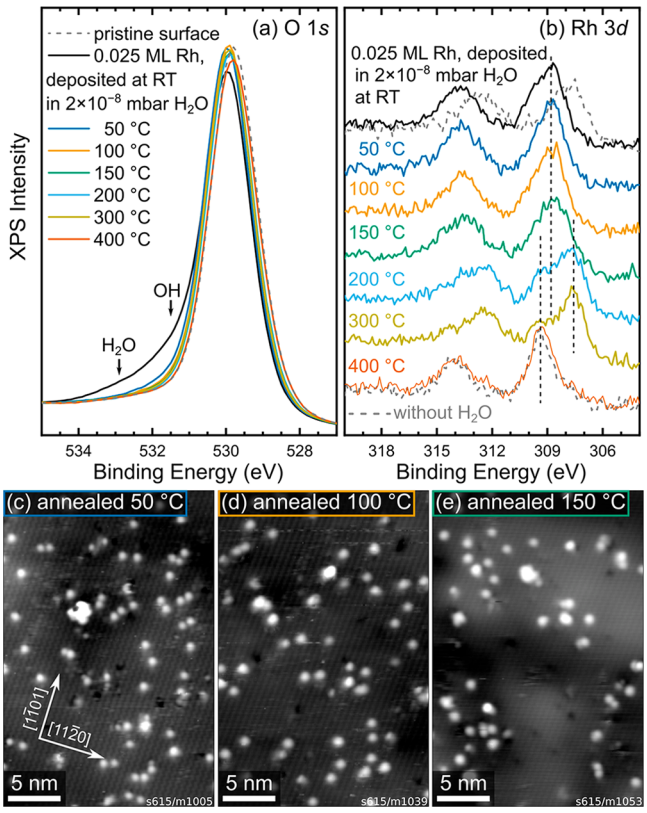

Figure 3. Thermal stability of H_2O-stabilized Rh on α-$Fe_2O_3(1\bar{1}02)$. (a and b) XPS data (Al Kα, 70° grazing emission, pass energy 16 eV) of the O 1s and Rh 3d regions, respectively, of 0.025 ML Rh deposited on α-$Fe_2O_3(1\bar{1}02)$ at room temperature in a partial pressure of 2×10^{-8} mbar H_2O and after successive annealing steps (10 min each) in UHV at different temperatures. The as-deposited spectra (black) correspond to the data shown in Figure 1b and Figure 2a. In panel b, corresponding spectra for the same Rh coverage, but deposited without H_2O, are shown for comparison (gray, dashed). The positions of the initial peak maximum (308.9 eV) and the two main components at elevated temperatures (307.6 and 309.3 eV) are marked by the vertical dashed lines. (c–e) STM images taken after the first three annealing steps, corresponding to the blue, orange, and green lines in panels a and b: (c) 50 °C (U_{sample} = +3 V, I_{tunnel} = 0.2 nA), (d) 100 °C (U_{sample} = +3 V, I_{tunnel} = 0.1 nA), and (e) 150 °C (U_{sample} = +3 V, I_{tunnel} = 0.1 nA).

heating to 100 °C and to noise level at higher temperatures. The O 1s peak then remains unchanged until Rh is fully incorporated at 400 °C, at which point the peak maximum shifts back to match the one of the pristine surface. The Rh 3d peak (Figure 3b) initially has its maximum at ∼308.9 eV, significantly higher than when Rh is deposited without water (307.8 eV, dashed gray line).[20] The maximum remains at this position while heating to 100 and 150 °C. At higher temperatures, the behavior closely resembles that previously observed in the absence of water: A component corresponding to clusters (307.6 eV) starts developing at 150 °C and reaches a maximum at 300 °C, and a component corresponding to incorporated Rh (309.3 eV) first appears at 200 °C and finally accounts for almost the entire Rh peak at 400 °C.[20]

In STM, most of the single features remain after annealing to 50 °C (Figure 3c), although some clusters are also visible. Interestingly, the single features differ from the state directly after deposition (Figure 1) in that they are immobile and do not exhibit the switching of apparent height observed at room temperature. In the absence of Rh, all water is already desorbed from the support at this temperature,[18] so the remaining OH visible in XPS is likely bound to the Rh adatoms. After heating to 100 and 150 °C (Figure 3d,e), the number of single features is reduced in each temperature step as Rh sinters to small clusters. Because almost no signature of OH or H_2O remains in XPS after heating to 100 °C, it seems plausible that at this point, sintering is limited purely by diffusion kinetics. Measuring only single features, we also find a slightly lower apparent height in STM after annealing to 100 °C [(152 ± 13) pm] than after annealing to 50 °C [(180 ± 19) pm]. Interestingly, while Rh deposited without water at room temperature sinters immediately, some single atoms remain even when most water has been desorbed. This may suggest that the temporary coordination to water facilitates a metastable configuration that is not directly accessible at room temperature in UHV, although we cannot exclude stabilization by trace OH groups still present near the XPS detection limit.

To further characterize the configuration of water-stabilized Rh on α-$Fe_2O_3(1\bar{1}02)$, we performed the same deposition in 2×10^{-8} mbar H_2O in a different UHV chamber, annealed the sample to remove the water not coordinated to Rh, then acquired ncAFM images with a CO-terminated tip at liquid-He temperature (∼4 K). The results are shown in Figure 4a. Two different motifs are observed, consisting of either two or three bright features on top of a darker area, marked by green and orange arrows, respectively. Both motifs also occur in a mirrored form, as expected based on the surface symmetry. In the absence of water, Rh adatoms are imaged as dark features in ncAFM at these scanning conditions, and we therefore assign the bright features to coadsorbed water. Considering the position of the features with respect to the underlying surface, we propose the model for the motif containing two bright features shown in Figure 4b. Here, Rh is coordinated in a square-planar geometry with two bonds to surface oxygen and two bonds to OH groups, which also bind to surface iron. Importantly, these OH groups sit at the same sites as water adsorbed on the pristine α-$Fe_2O_3(1\bar{1}02)$ surface.[18] It seems likely that an additional water molecule can be added at one end of the complex, resulting in an HO–H_2O configuration characteristic of water adsorbed on α-$Fe_2O_3(1\bar{1}02)$ in the absence of Rh.[18] This would explain the motifs consisting of three bright features, marked by orange arrows in Figure 4a. In principle, the Rh adatom may also form an additional bond to a lattice oxygen atom below it, as indicated in Figure S4b. However, because that oxygen atom is already in a bulk-like 4-fold coordination environment, we assume that such a bond would be significantly weaker and would have only minor effects on the overall Rh stability.

The assumption of two OH groups coordinated to each Rh adatom fits with the OH contribution in XPS (Figure S2) if approximately six substrate oxygen layers contribute to the XPS signal. This would correspond to a probing depth of 5.9 Å and an electron path length in the crystal of 17.3 Å at 70° grazing emission, which is on the order of magnitude of the inelastic mean free path, estimated as ∼20 Å at $E_{kin} \approx$ 950 eV.[21,22] Therefore, although experimental and theoretical uncertainties do not allow direct determination of the OH coverage from XPS, the proposed model plausibly fits the XPS O 1s data.

https://doi.org/10.1021/acsenergylett.1c02405
ACS Energy Lett. 2022, 7, 375–380

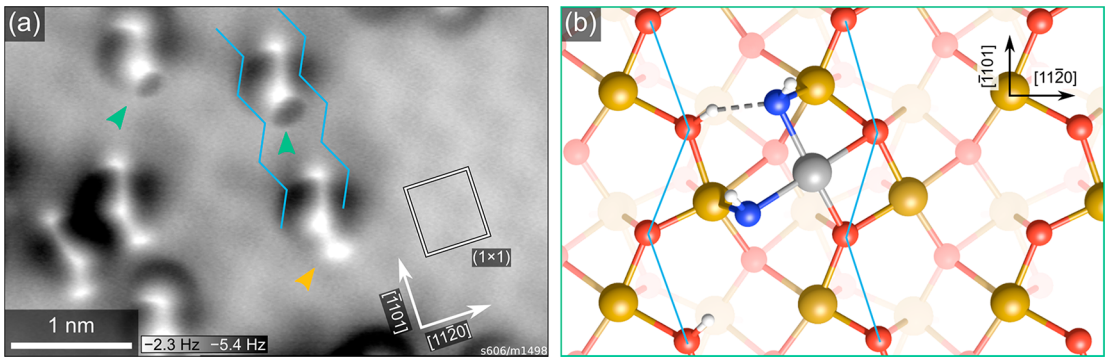

Figure 4. Structure of H_2O-stabilized Rh on α-$Fe_2O_3(1\bar{1}02)$. (a) ncAFM image acquired at liquid He temperature of 0.05 ML Rh on α-$Fe_2O_3(1\bar{1}02)$, deposited at room temperature in a partial pressure of 2×10^{-8} mbar H_2O, then heated to 80 °C to desorb all water not coordinated to Rh. (b) Schematic model (top view) for the features indicated by green arrows in panel a. A Rh adatom (gray) is stabilized by two OH groups (O_{water} in blue, hydrogen in white). The zigzag rows of surface oxygen are marked in blue in both panels. The orange arrow highlights a third protrusion that is sometimes present, which we tentatively attribute to an additional water molecule atop a surface Fe and hydrogen-bonded to one of the OH groups. Additional side and perspective views of the model in panel b are shown in Figure S4.

Overall, our data show that single Rh adatoms are stabilized on α-$Fe_2O_3(1\bar{1}02)$ in the presence of water. Interestingly, it appears that two different stabilization mechanisms are at work depending on the water coverage. When Rh is deposited, a complete monolayer of water is likely present on the surface. Under these conditions, we find that the adatoms are mobile, but do not agglomerate, indicating thermodynamic stabilization, i.e., single atoms are energetically more favorable than dimers. Using the direct ncAFM imaging of the adsorbed $Rh(OH)_x$ complex (Figure 4), we can rationalize this stability through the square-planar coordination of the adatoms, which is expected to be favorable by analogy to Rh coordination complexes. This was previously observed for Rh and Ir adatoms on $Fe_3O_4(001)$.[23,24] Because the two OH ligands are located in the same sites as water adsorbed at room temperature on the pristine α-$Fe_2O_3(1\bar{1}02)$ surface,[18] no rearrangement is required to accommodate ad-Rh species as they are deposited. The facile diffusion of adatoms after deposition may be explained by Rh diffusing underneath the water ad-layer, as Rh can be handed over to neighboring OH groups. In contrast, once the surrounding water is desorbed, diffusion requires displacing the entire $Rh(OH)_x$ complex at once, breaking not only the Rh−O(H) bonds but also the bonds of OH to surface Fe, thus likely resulting in higher diffusion barriers.

The switching of apparent height observed in STM (Figure 1a) is most likely because of adsorption and desorption of either (i) molecules from the residual gas or the STM tip or (ii) molecular H_2O from the surface. In contrast to incorporated 6-fold coordinated Rh, which form after annealing in O_2,[20] these adatoms thus have the capability to act as reaction centers. In the model shown in Figure 4b, we speculate that binding another ligand may allow the Rh adatom to switch from a square-planar to an octahedral coordination by forming an additional bond with the surface oxygen atom directly below it (initial distance ≈ 2.3 Å in the structure as drawn; see Figure S4). If this process is facile, it would be conceptually similar to Wilkinson's catalyst, in which Rh switches between square-planar and octahedral coordination. In general, while single atoms stabilized entirely through coordination to lattice oxygen tend to be catalytically inactive,[25] we can expect stabilization of adatoms through OH groups to allow for more dynamic reaction kinetics because the adatoms are less strongly oxidized and the ligands easier to displace. Moreover, coordination to OH groups likely allows more flexibility in the structure than the rigid oxide lattice.

In addition to stabilizing the adatoms in an active geometry, the presence of water may also directly contribute to reaction pathways, as proposed for low-temperature CO oxidation on the Au/TiO_2 system.[14] Even more substantial involvement has been demonstrated for Pt_1/CeO_2, where water oxygen is used for CO oxidation via an intermediate step in a Mars−van Krevelen (MvK) process.[13] It seems plausible that similar abstraction of oxygen from OH groups may be relevant more generally, especially when MvK pathways have been proposed to explain oxidation pathways at or near room temperature occurring on substrates with high oxygen vacancy formation energies.

The high XPS core-level binding energy observed here for Rh 3d (Figure 3b) indicates that the electronic structure of the adatoms is also strongly modified by their coordination to water. Clearly, any change to the Rh oxidation state would also affect its interaction with reactants, affecting both infrared frequencies and reaction barriers. A similar effect was previously proposed for Rh adatoms interacting with OH groups on anatase TiO_2.[12] However, this Rh−OH configuration on anatase occurred only after reduction treatment in H_2 gas.[12] In contrast, dissociated water is stably adsorbed on the α-$Fe_2O_3(1\bar{1}02)$ surface at room temperature, and favorable adsorption sites for Rh adatoms are available even without rearranging the water overlayer; therefore, an Rh−OH configuration is expected to occur in most realistic conditions. Our results therefore strongly suggest that coadsorption of water must be accounted for in theoretical studies to accurately model reaction pathways.

EXPERIMENTAL METHODS

Room-temperature STM and XPS results were collected in a UHV setup consisting of a preparation chamber (base pressure < 10^{-10} mbar) and an analysis chamber (base pressure < 5×10^{-11} mbar). This system is equipped with a non-monochromatic Al Kα X-ray source (VG), a SPECS Phoibos 100 analyzer for XPS, and an Omicron μ-STM. The STM was operated in constant-current mode using electrochemically etched W tips. STM images were corrected for distortion and

https://doi.org/10.1021/acsenergylett.1c02405
ACS Energy Lett. 2022, 7, 375−380

creep of the piezo scanner, as described in ref 26. Apparent heights of adatom features were measured with respect to the mean height of a ∼3 nm-diameter ring around the feature of interest. Noncontact AFM results were acquired in a separate UHV setup using an Omicron LT-STM equipped with a QPlus sensor and an in-vacuum preamplifier.[27] Rh was deposited from a rod with an electron-beam evaporator (Focus), using a quartz-crystal microbalance to calibrate the deposition rate, with deposition times of ca. 30−120 s for 0.025−0.1 monolayers (ML) of rhodium. A repelling bias of +1.1 kV was applied to a cylindrical electrode at the orifice during deposition to avoid implantation of Rh ions. Throughout this Letter, we define a monolayer as the number of Fe atoms in the surface layer. One ML of Rh is therefore defined as two Rh atoms per α-$Fe_2O_3(1\bar{1}02)$-(1 × 1) unit cell, which corresponds to a density of 7.3×10^{14} atoms cm^{-2}. The evaporation rate was always calibrated in UHV, even when the deposition was carried out in a background of H_2O, which results in errors in the actual coverages. The nominal coverages given in this work are not corrected for these errors and probably overestimate the Rh coverage (see Figure S3). When depositing Rh with a background of water, the sample was always first exposed to 2 L H_2O (1 L = 1.33×10^{-6} mbar × s) to ensure a constant H_2O coverage during the deposition.

The experiments were conducted on single-crystalline, 0.03 atom % Ti-doped hematite films grown homoepitaxially by pulsed laser deposition on natural α-$Fe_2O_3(1\bar{1}02)$ samples (SurfaceNet GmbH, 10 × 10 × 0.5 mm^3, <0.3° miscut), as described in detail elsewhere.[19,20] This ensures sufficient conductivity of the samples for STM without reducing the oxide. The surface appears identical to the undoped samples studied previously.[17] Before each experiment, the sample was reprepared by sputtering (1 keV Ar^+ ions, ∼2 μA, 15 min) and annealing in oxygen (2×10^{-6} mbar, 520 °C) for 30 min.

■ ASSOCIATED CONTENT

Supporting Information

The Supporting Information is available free of charge at https://pubs.acs.org/doi/10.1021/acsenergylett.1c02405.

Additional figures illustrating the structure of the clean surface, room-temperature water adsorption sites, and the $Rh(OH)_x$ model; fits to XPS O 1s data shown in Figure 2; STM images of Rh deposited in H_2O background before and after incorporation and description of the coverage quantification (PDF)

■ AUTHOR INFORMATION

Corresponding Author

Gareth S. Parkinson − *Institute of Applied Physics, TU Wien, 1040 Wien, Austria;* orcid.org/0000-0003-2457-8977; Email: parkinson@iap.tuwien.ac.at

Authors

Florian Kraushofer − *Institute of Applied Physics, TU Wien, 1040 Wien, Austria;* orcid.org/0000-0003-1314-9149

Lena Haager − *Institute of Applied Physics, TU Wien, 1040 Wien, Austria*

Moritz Eder − *Chair of Physical Chemistry & Catalysis Research Center, Technical University of Munich, 85748 Garching, Germany*

Ali Rafsanjani-Abbasi − *Institute of Applied Physics, TU Wien, 1040 Wien, Austria;* orcid.org/0000-0001-9155-7848

Zdeněk Jakub − *Institute of Applied Physics, TU Wien, 1040 Wien, Austria;* orcid.org/0000-0001-9538-9087

Giada Franceschi − *Institute of Applied Physics, TU Wien, 1040 Wien, Austria;* orcid.org/0000-0003-3525-5399

Michele Riva − *Institute of Applied Physics, TU Wien, 1040 Wien, Austria;* orcid.org/0000-0001-8303-7383

Matthias Meier − *Institute of Applied Physics, TU Wien, 1040 Wien, Austria*

Michael Schmid − *Institute of Applied Physics, TU Wien, 1040 Wien, Austria*

Ulrike Diebold − *Institute of Applied Physics, TU Wien, 1040 Wien, Austria;* orcid.org/0000-0003-0319-5256

Complete contact information is available at: https://pubs.acs.org/10.1021/acsenergylett.1c02405

Notes

The authors declare no competing financial interest.

■ ACKNOWLEDGMENTS

G.S.P., F.K., L.H., M.M., and A.R.-A. acknowledge funding from the European Research Council (ERC) under the European Union's Horizon 2020 research and innovation programme (Grant Agreement No. 864628). Z.J. was supported by the Austrian Science Fund (FWF, Y847-N20, START Prize). G.F. and U.D. acknowledge funding from the European Research Council (ERC) under the European Union's Horizon 2020 research and innovation programme (Grant Agreement No. 883395, Advanced Research Grant "WatFun"). M.E. acknowledges support from the TUM-GS of the TU Munich.

■ REFERENCES

(1) Qiao, B.; Wang, A.; Yang, X.; Allard, L. F.; Jiang, Z.; Cui, Y.; Liu, J.; Li, J.; Zhang, T. Single-atom catalysis of CO oxidation using Pt_1/FeO_x. *Nat. Chem.* **2011**, *3* (8), 634−641.

(2) Liang, J.-X.; Lin, J.; Yang, X.-F.; Wang, A.-Q.; Qiao, B.-T.; Liu, J.; Zhang, T.; Li, J. Theoretical and Experimental Investigations on Single-Atom Catalysis: Ir_1/FeO_x for CO Oxidation. *J. Phys. Chem. C* **2014**, *118* (38), 21945−21951.

(3) Shi, Y.; Zhao, C.; Wei, H.; Guo, J.; Liang, S.; Wang, A.; Zhang, T.; Liu, J.; Ma, T. Single-Atom Catalysis in Mesoporous Photovoltaics: The Principle of Utility Maximization. *Adv. Mater.* **2014**, *26* (48), 8147−8153.

(4) Wei, H.; Liu, X.; Wang, A.; Zhang, L.; Qiao, B.; Yang, X.; Huang, Y.; Miao, S.; Liu, J.; Zhang, T. FeO_x-supported platinum single-atom and pseudo-single-atom catalysts for chemoselective hydrogenation of functionalized nitroarenes. *Nat. Commun.* **2014**, *5* (1), 5634.

(5) Rossell, M. D.; Caparrós, F. J.; Angurell, I.; Muller, G.; Llorca, J.; Seco, M.; Rossell, O. Magnetite-supported palladium single-atoms do not catalyse the hydrogenation of alkenes but small clusters do. *Catal. Sci. Technol.* **2016**, *6* (12), 4081−4085.

(6) Liu, J. Catalysis by Supported Single Metal Atoms. *ACS Catal.* **2017**, *7* (1), 34−59.

(7) Zhao, Y.; Yang, K. R.; Wang, Z.; Yan, X.; Cao, S.; Ye, Y.; Dong, Q.; Zhang, X.; Thorne, J. E.; Jin, L.; Materna, K. L.; Trimpalis, A.; Bai, H.; Fakra, S. C.; Zhong, X.; Wang, P.; Pan, X.; Guo, J.; Flytzani-Stephanopoulos, M.; Brudvig, G. W.; Batista, V. S.; Wang, D. Stable iridium dinuclear heterogeneous catalysts supported on metal-oxide substrate for solar water oxidation. *Proc. Natl. Acad. Sci. U. S. A.* **2018**, *115* (12), 2902−2907.

(8) Li, F.; Li, Y.; Zeng, X. C.; Chen, Z. Exploration of High-Performance Single-Atom Catalysts on Support M_1/FeO_x for CO

Oxidation via Computational Study. *ACS Catal.* **2015**, *5* (2), 544−552.
(9) Qiao, B.; Liang, J.-X.; Wang, A.; Xu, C.-Q.; Li, J.; Zhang, T.; Liu, J. J. Ultrastable single-atom gold catalysts with strong covalent metal-support interaction (CMSI). *Nano Research* **2015**, *8* (9), 2913−2924.
(10) Liang, J.; Yu, Q.; Yang, X.; Zhang, T.; Li, J. A systematic theoretical study on FeO_x-supported single-atom catalysts: M_1/FeO_x for CO oxidation. *Nano Research* **2018**, *11* (3), 1599−1611.
(11) Liang, J.-X.; Lin, J.; Liu, J.; Wang, X.; Zhang, T.; Li, J. Dual Metal Active Sites in an Ir_1/FeO_x Single-Atom Catalyst: A Redox Mechanism for the Water-Gas Shift Reaction. *Angew. Chem., Int. Ed.* **2020**, *59* (31), 12868−12875.
(12) Asokan, C.; Thang, H. V.; Pacchioni, G.; Christopher, P. Reductant composition influences the coordination of atomically dispersed Rh on anatase TiO_2. *Catal. Sci. Technol.* **2020**, *10* (6), 1597−1601.
(13) Wang, C.; Gu, X.-K.; Yan, H.; Lin, Y.; Li, J.; Liu, D.; Li, W.-X.; Lu, J. Water-Mediated Mars−Van Krevelen Mechanism for CO Oxidation on Ceria-Supported Single-Atom Pt_1 Catalyst. *ACS Catal.* **2017**, *7* (1), 887−891.
(14) Saavedra, J.; Doan, H. A.; Pursell, C. J.; Grabow, L. C.; Chandler, B. D. The critical role of water at the gold-titania interface in catalytic CO oxidation. *Science* **2014**, *345* (6204), 1599−1602.
(15) Kuhlenbeck, H.; Shaikhutdinov, S.; Freund, H.-J. Well-Ordered Transition Metal Oxide Layers in Model Catalysis − A Series of Case Studies. *Chem. Rev.* **2013**, *113* (6), 3986−4034.
(16) Parkinson, G. S. Iron oxide surfaces. *Surf. Sci. Rep.* **2016**, *71* (1), 272−365.
(17) Kraushofer, F.; Jakub, Z.; Bichler, M.; Hulva, J.; Drmota, P.; Weinold, M.; Schmid, M.; Setvin, M.; Diebold, U.; Blaha, P.; Parkinson, G. S. Atomic-Scale Structure of the Hematite α-$Fe_2O_3(1\bar{1}02)$ "R-Cut" Surface. *J. Phys. Chem. C* **2018**, *122* (3), 1657−1669.
(18) Jakub, Z.; Kraushofer, F.; Bichler, M.; Balajka, J.; Hulva, J.; Pavelec, J.; Sokolovic, I.; Mullner, M.; Setvin, M.; Schmid, M.; Diebold, U.; Blaha, P.; Parkinson, G. S. Partially Dissociated Water Dimers at the Water-Hematite Interface. *ACS Energy Lett.* **2019**, *4* (2), 390−396.
(19) Franceschi, G.; Kraushofer, F.; Meier, M.; Parkinson, G. S.; Schmid, M.; Diebold, U.; Riva, M. A Model System for Photocatalysis: Ti-Doped α-$Fe_2O_3(1\bar{1}02)$ Single-Crystalline Films. *Chem. Mater.* **2020**, *32* (9), 3753−3764.
(20) Kraushofer, F.; Resch, N.; Eder, M.; Rafsanjani-Abbasi, A.; Tobisch, S.; Jakub, Z.; Franceschi, G.; Riva, M.; Meier, M.; Schmid, M.; Diebold, U.; Parkinson, G. S. Surface Reduction State Determines Stabilization and Incorporation of Rh on α-$Fe_2O_3(1\bar{1}02)$. *Adv. Mater. Interfaces* **2021**, *8* (8), 2001908.
(21) Seah, M. P.; Dench, W. A. Quantitative electron spectroscopy of surfaces: A standard data base for electron inelastic mean free paths in solids. *Surf. Interface Anal.* **1979**, *1* (1), 2−11.
(22) Smekal, W.; Werner, W. S.; Powell, C. J. Simulation of electron spectra for surface analysis (SESSA): a novel software tool for quantitative Auger-electron spectroscopy and X-ray photoelectron spectroscopy. *Surf. Interface Anal.* **2005**, *37* (11), 1059−1067.
(23) Jakub, Z.; Hulva, J.; Meier, M.; Bliem, R.; Kraushofer, F.; Setvin, M.; Schmid, M.; Diebold, U.; Franchini, C.; Parkinson, G. S. Local Structure and Coordination Define Adsorption in a Model Ir_1/Fe_3O_4 Single-Atom Catalyst. *Angew. Chem.* **2019**, *131* (39), 14099−14106.
(24) Jakub, Z.; Hulva, J.; Ryan, P. T.; Duncan, D. A.; Payne, D. J.; Bliem, R.; Ulreich, M.; Hofegger, P.; Kraushofer, F.; Meier, M.; et al. Adsorbate-induced structural evolution changes the mechanism of CO oxidation on a $Rh/Fe_3O_4(001)$ model catalyst. *Nanoscale* **2020**, *12* (10), 5866−5875.
(25) Lykhach, Y.; Bruix, A.; Fabris, S.; Potin, V.; Matolínová, I.; Matolín, V.; Libuda, J.; Neyman, K. M. Oxide-based nanomaterials for fuel cell catalysis: the interplay between supported single Pt atoms and particles. *Catal. Sci. Technol.* **2017**, *7* (19), 4315−4345.
(26) Choi, J.; Mayr-Schmölzer, W.; Mittendorfer, F.; Redinger, J.; Diebold, U.; Schmid, M. The growth of ultra-thin zirconia films on $Pd_3Zr(0001)$. *J. Phys.: Condens. Matter* **2014**, *26* (22), 225003.
(27) Huber, F.; Giessibl, F. J. Low noise current preamplifier for qPlus sensor deflection signal detection in atomic force microscopy at room and low temperatures. *Rev. Sci. Instrum.* **2017**, *88* (7), 073702.

https://doi.org/10.1021/acsenergylett.1c02405
ACS Energy Lett. 2022, 7, 375−380